

# UNVEILING AI’S BLIND SPOTS: AN ORACLE FOR IN-DOMAIN, OUT-OF-DOMAIN, AND ADVERSARIAL ERRORS

Shuangpeng Han<sup>1,2</sup>, Mengmi Zhang<sup>1,2,\*</sup>

<sup>1</sup>College of Computing and Data Science, Nanyang Technological University, Singapore

<sup>2</sup>Deep NeuroCognition Lab, I2R and CFAR, Agency for Science, Technology and Research (A\*STAR)

## ABSTRACT

AI models make mistakes when recognizing images—whether in-domain, out-of-domain, or adversarial. Predicting these errors is critical for improving system reliability, reducing costly mistakes, and enabling proactive corrections in real-world applications such as healthcare, finance, and autonomous systems. However, understanding what mistakes AI models make, why they occur, and how to predict them remains an open challenge. Here, we conduct comprehensive empirical evaluations using a "mentor" model—a deep neural network designed to predict another model’s errors. Our findings show that the mentor model excels at learning from a mentee’s mistakes on adversarial images with small perturbations and generalizes effectively to predict in-domain and out-of-domain errors of the mentee. Additionally, transformer-based mentor models excel at predicting errors across various mentee architectures. Subsequently, we draw insights from these observations and develop an "oracle" mentor model, dubbed SuperMentor, that achieves 78% accuracy in predicting errors across different error types. Our error prediction framework paves the way for future research on anticipating and correcting AI model behaviours, ultimately increasing trust in AI systems. All code, models, and data will be made publicly available.

## 1 INTRODUCTION

AI models are prone to making errors in image recognition tasks, whether dealing with in-domain, out-of-domain (OOD), or adversarial examples. In-domain errors occur when models misclassify familiar data within the training domain, while OOD errors arise when faced with unseen or out-of-domain data. Adversarial errors are particularly concerning, as they result from carefully crafted perturbations designed to mislead the model.

Accurately predicting these errors is critical to enhancing the overall robustness and reliability of AI systems, especially in high-stakes real-world applications such as healthcare (Habehh & Gohel, 2021), finance (Mashrur et al., 2020), and autonomous driving (Huang et al., 2022). Proactively identifying potential errors enables more efficient corrections, reducing costly mistakes and safeguarding against catastrophic failures. By predicting when models are likely to err, we can implement strategies that either mitigate or entirely avoid the risks associated with those errors, ultimately leading to more trustworthy AI deployments.

Understanding the specific types of errors AI systems make, the reasons why they make these errors, and most importantly, how to predict these errors remains an unresolved challenge. Existing literature on error monitoring systems for AI models encompasses various approaches, including uncertainty estimation (Nado et al., 2021; Lakshminarayanan et al., 2017), anomaly detection (Bogdoll et al., 2022), outlier detection (Boukerche et al., 2020), and out-of-domain detection (Yang et al., 2024). While these methods are crucial for assessing model reliability, they mainly focus on determining whether a given data point falls outside the scope of the model’s training. Thus, these approaches misalign with our primary objective of predicting whether AI models will make mistakes, as models can err on familiar data while behaving correctly on out-of-scope samples.

\*Corresponding author; address correspondence to mengmi.zhang@ntu.edu.sg

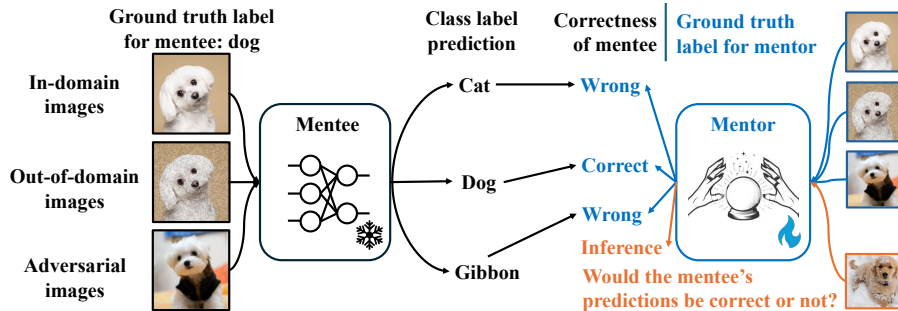


Figure 1: **AI models make mistakes and an "oracle" mentor model predicts when they will happen.** A "mentee" neural network (black) was trained for multi-class image recognition, but it can still misclassify in-domain, out-of-domain, and adversarial images. For instance, it might mislabel an in-domain dog image as a cat. The mentor model (blue), inputting the same images as the mentee, predicts whether the mentee will make a mistake. For example, if the mentee incorrectly labels an adversarial dog image, the mentor's ground truth label is "wrong"; conversely, if the mentee correctly labels an out-of-domain dog image, the mentor's label is "correct". The mentee's parameters are frozen (snowflake), while the mentor's are trainable (fire). During inference (orange), the mentor predicts whether the mentee will make an error on test images that have never been seen by both the mentee and the mentor.

Subsequent research in out-of-domain detection has demonstrated that a model's accuracy is often correlated with how far the data deviates from in-domain samples (Hendrycks & Dietterich, 2019; Shankar et al., 2021; Li et al., 2017). These methods typically rely on predefined metrics, such as model parameter distances (Yu et al., 2022), model disagreements (Jiang et al., 2021; Madani et al., 2004) and confidence scores (Guillory et al., 2021), which limits their ability to generalize predictions across various data types, including errors arising from in-domain data or adversarial attacks (Szegedy, 2013). Another line of research improves the robustness of the AI models with adversarial training approaches (Ilyas et al., 2019; Goyal et al., 2020; Balunović & Vechev, 2020); however, these approaches primarily focus on improving the model's overall performance rather than predicting when errors may occur in the models.

Different from all these previous works, we delve into the underlying principles of errors generated by AI models in the task of image classification with another AI model. Specifically, we designate the AI model that predicts errors as the **mentor** and the AI model being evaluated for performance as the **mentee**. The mentor strives to predict whether the mentee makes a mistake for any given test data. See Fig. 1 for the detailed illustration of the problem setup. Training the mentor on the error patterns made by the mentee can potentially reveal the strengths and weaknesses of the mentee's learned representations across various visual contexts.

Specifically, we examine the effects of three distinct error types AI models often make: In-Domain (ID) Errors, Out-of-Domain (OOD) Errors, and Adversarial Attack (AA) Errors on three increasingly complex image datasets CIFAR-10 (Krizhevsky et al., 2009), CIFAR-100 (Krizhevsky et al., 2009) and ImageNet-1K (Deng et al., 2009). We identify which of these error types has the most significant impact on the mentor's error prediction performances, and explore the reasons behind its prominence. Additionally, we assess how different mentor architectures influence error prediction accuracy and evaluate the mentor's generalization performance across various mentee architectures. Finally, we develop a SuperMentor model that successfully predicts errors of the mentee with 78% accuracy across diverse error types. Our main contributions are highlighted below:

1. We conduct an in-depth analysis of how training mentors on each of three distinct error types specified by the mentees—In-Domain (ID) Errors, Out-of-Domain (OOD) Errors, and Adversarial Attack (AA) Errors—affect the performance of error predictions over three increasingly complex image datasets. Our results reveal that training mentors with adversarial attack errors from the mentee has the most significant impact on improving the mentor's error prediction accuracy.
2. We explore how various mentor model architectures affect error prediction performance. Our experiments demonstrate that transformer-based mentor models outperform other architectures in accurately predicting errors.

3. We investigate how varying levels of distortion in OOD and adversarial images affect the accuracy of error predictions. The findings indicate that training mentors with images with small perturbations can improve error prediction accuracy. In addition, we show that a mentor trained to learn error patterns from one mentee can successfully generalize its error predictions to another mentee.

4. Based on our findings from points 1 to 3, we present the SuperMentor model, which predicts errors across diverse mentee architectures and error types. Experimental results show that SuperMentor outperforms baseline mentors, demonstrating its superior error-predictive capabilities.

## 2 RELATED WORK

**Error monitoring systems for AI models.** With the growing deployment of AI models across diverse fields, ensuring their reliability and understanding their limitations has become increasingly crucial. This has led to numerous research in safe AI such as uncertainty estimation (Nado et al., 2021; Lakshminarayanan et al., 2017), anomaly detection (Bogdoll et al., 2022), outlier detection (Boukerche et al., 2020), and out-of-domain detection (Yang et al., 2024). Unlike these areas, which mainly aim to predict whether the input data falls outside the training domain, our focus is on monitoring and predicting errors in AI models by determining whether the model’s output is correct, irrespective of whether the data comes from the training domain.

Moreover, to detect whether the input data is out of scope, the prior approaches mainly rely on softmax outputs (Granese et al., 2021; Hendrycks & Gimpel, 2016; Dang et al., 2024) or activations from network layers (Wang et al., 2020; Cheng et al., 2019; Ferreira et al., 2023), in applications such as object detection (Kang et al., 2018) and trajectory prediction (Shao et al., 2023; 2024). However, these methods often depend on manually defined metrics to estimate the probability of a mentee making a mistake. In contrast, our approach leverages another AI model to automatically learn and approximate the mentee’s decision boundaries, predicting its errors in an end-to-end trainable manner.

**Out-of-domain detection.** Our research on predicting mentee errors is closely related to out-of-domain detection in error monitoring systems, though it differs in several key aspects. As highlighted by (Guérin et al., 2023), error prediction is distinct from OOD detection (Liu et al., 2020a; Sun et al., 2021; Lee et al., 2018; Sun et al., 2022) in their objectives. While OOD detection aims to detect whether the given data comes from the same domain as the training set, the aim of error prediction is to learn whether the mentee will make a mistake on the given data. In other words, out-of-domain data may not necessarily cause the model to err, and model errors can also occur on in-domain data.

Recent studies (Hendrycks & Dietterich, 2019; Shankar et al., 2021; Li et al., 2017) have shown that a model’s accuracy on a given dataset is often correlated with how far the data deviates from in-domain samples. However, these studies typically rely on pre-defined metrics, such as model parameter distances (Yu et al., 2022), model disagreements (Jiang et al., 2021; Madani et al., 2004), confidence scores (Guillory et al., 2021), domain-invariant representations (Chuang et al., 2020), and domain augmentation (Deng et al., 2021a), limiting their ability to generalize error prediction for in-domain data. In contrast, our mentor model is capable of predicting both OOD and in-domain errors for a mentee. Additionally, our mentor is an AI model trained end-to-end, eliminating the need for manually defined criteria.

**Adversarial attack and defense.** In addition to OOD error, (Szegedy, 2013) discovered that deep neural networks can be fooled using input perturbations of extremely low magnitude. Building upon this finding, a substantial number of adversarial attacks have been proposed, including white-box attacks (Goodfellow et al., 2014; Mađry et al., 2017; Carlini & Wagner, 2017; Schwinn et al., 2023; Gao et al., 2020), black-box attacks (Uesato et al., 2018; Rahmati et al., 2020; Brendel et al., 2017; Chen et al., 2020), and backdoor attacks (Liu et al., 2020b; Xie et al., 2019; Kolouri et al., 2020). To defend against these adversarial attacks, various defence mechanisms (Qin et al., 2019; Deng et al., 2021b; Liu et al., 2019) have been developed to withstand or detect adversarial inputs. Furthermore, although the primary objective of adversarial attacks is to deceive AI models, there are instances where adversarial perturbations are exploited to enhance the model performance — a technique known as adversarial training (Ilyas et al., 2019; Goyal et al., 2020; Balunović & Vechev, 2020). Unlike adversarial training, which involves using adversarial samples to train the mentee, our approach focuses on teaching mentors to learn the mentee’s error patterns revealed by these adversarial attack samples.

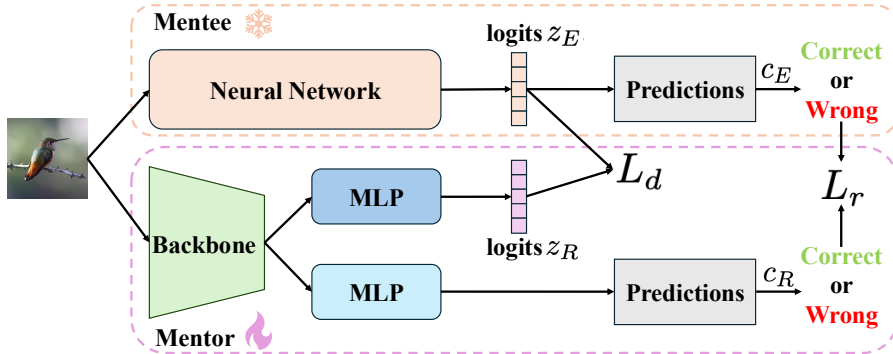


Figure 2: **Overview of a mentor model.** Given a fixed mentee model (snowflake), the mentor model takes an input image and uses a pre-trained backbone on ImageNet-1K (Deng et al., 2009) to extract features. The feature maps are then processed in two streams via multi-layer perceptrons (MLP)s. The output logits  $z_R$  from one stream are compared with the mentee’s output logits  $z_E$  using a distillation loss  $L_d$ . The other stream performs a binary prediction of whether the mentee makes a mistake or not. The prediction is supervised by a logistic regression loss  $L_r$ . The parameters of MLPs in the two streams are not shared.

### 3 EXPERIMENTAL SETUPS

We denote the mentor and mentee networks as  $f_R(\cdot)$  and  $f_E(\cdot)$  respectively. We also define  $\mathcal{X}$  as the domain-specific set containing all the test images for a mentee, and  $\mathcal{Y}$  as their ground-truth object class labels. Therefore, a mentor is expected to make perfect predictions about the correctness of the mentee’s responses (1 for "correct" and 0 for "wrong") given any image  $x$  from  $\mathcal{X}$ :

$$\forall x \in \mathcal{X}, f_R(x) = \begin{cases} 1, & \text{if } f_E(x) = y, \\ 0, & \text{otherwise} \end{cases} \quad (1)$$

where  $y \in \mathcal{Y}$  is the ground-truth object class label of the corresponding image  $x$ .

#### 3.1 MENTORS

**Model Architecture:** We propose mentor models, as illustrated in **Fig. 2**. Given an input image, the backbone of a mentor model extracts features from the input image. We adopt either of the two backbones for the feature extractors of mentors: a 2D Convolutional Neural Network (2D-CNN) ResNet50 (He et al., 2016) and a transformer-based ViT (Dosovitskiy, 2020). The extracted feature maps are further processed in two streams implemented as multi-layer perceptrons (MLP)s. The parameters of the MLPs in the two streams are not shared.

The first stream generates logits  $z_R$  by predicting the probability distribution of a mentee over all the object classes when the mentee classifies the given image. The mentee network is kept fixed while training the mentor. Let us define the mentee’s output logit as  $z_E$ . We introduce the distillation loss proposed by (Hinton, 2015):  $L_d = \text{Distill}(z_R, z_E)$  to align  $z_R$  with  $z_E$ . We set the temperature hyper-parameter in  $L_d$  as 1.0, which controls the smoothness of the soft probability distribution. Higher temperatures make the distribution softer and more uniform across classes.

In the second stream, the mentor is prompted to predict whether the mentee will make a mistake on the given image or not. We denote the predicted binary label as  $c_R$ , where 1 indicates that the mentee does not make a mistake and vice versa for 0. This prediction is supervised by  $L_r = \text{LR}(c_R, c_E)$  where  $\text{LR}(\cdot, \cdot)$  is the logistic regression loss and  $c_E$  is the ground truth correctness label of a mentee. The overall loss is  $L = L_d + L_r$ .

**Training and Implementation Details:** All mentors are trained on Nvidia RTX A5000 and A6000 GPUs, utilizing the AdamW optimizer (Loshchilov & Hutter, 2017) with a cosine annealing scheduler (Loshchilov & Hutter, 2016), and an initial learning rate of  $2 \times 10^{-4}$ . All mentors load the weights of the feature extractor pre-trained on the ImageNet-1K dataset for 1000-way image classification tasks (Deng et al., 2009) and further fine-tune on the error prediction task. During training, images

are resized and center-cropped to  $224 \times 224$  pixels. All the mentor models are trained for 40 epochs with a batch size of 512.

### 3.2 MENTEES AND THEIR DATASETS

We employ two architectures as the mentees’ backbones: ResNet50 (He et al., 2016), which is a 2D-Convolutional neural network (2D-CNN), and ViT (Dosovitskiy, 2020), which is a transformer architecture based on self-attention mechanisms.

To train and test our mentees, we include three prominent image datasets of varying sizes and follow their standard data splits: CIFAR-10 (C10, (Krizhevsky et al., 2009)) with 10 object classes, CIFAR-100 with 100 object classes (C100, (Krizhevsky et al., 2009)) and ImageNet-1K with 1000 object classes (IN, (Deng et al., 2009)). Their multi-class recognition accuracy on the standard test sets of C10, C100 and IN datasets are 96.98%, 84.54%, 76.13% for the ResNet50 mentee and 97.45%, 86.51%, 81.07% for the ViT mentee respectively. The parameters of the mentees are frozen throughout all the experiments conducted on mentors.

### 3.3 DATASETS FOR TRAINING AND TESTING MENTORS

The mentor’s objective is to predict whether the mentee will misclassify a given image, regardless of its source. The mentor is trained on correctly and wrongly classified images by a mentee. Next, we introduce how these images are curated and collected.

A mentee may encounter various types of errors when dealing with real-world data. To explore which error types most effectively reveal the mentee’s learning patterns, we categorize errors into three types: (1) errors from in-domain test images, (2) errors from out-of-domain images, and (3) errors from adversarial images generated using adversarial attack methods. Next, we introduce these three error types in detail.

**In-Domain (ID) Errors.** occur on data that come from the same domain as the mentee’s training dataset. Specifically, errors on images from the standard validation set of ImageNet-1K or the test sets of CIFAR-10 and CIFAR-100 are considered ID errors. Along with the correctly classified images from these standard test sets, we create three datasets for a mentor: **IN-ID**, **C10-ID**, and **C100-ID**, following the naming convention of [Dataset]-[Error Type].

**Out-of-domain (OOD) Errors.** refer to errors that arise when the mentee encounters data outside the training domain. To obtain OOD samples of a dataset, we adopt four types of image corruptions from (Hendrycks & Dietterich, 2019): **speckle noise (SpN)** (noise category), **Gaussian blur (GaB)** (blur category), **spatter (Spat)** (weather category), and **saturate (Sat)** (digital category). The noise levels can vary and we select level 1 for image corruptions as specified in (Hendrycks & Dietterich, 2019) by default. As noise levels increase, the distortions on OOD images become more pronounced, leading to more mistakes of a mentee.

Following the naming conventions of [Dataset]-[Error Type]-[Error Source], we collect correctly and wrongly classified OOD samples based on C10 images of a mentee and curate four datasets for a mentor: **C10-OOD-SpN**, **C10-OOD-GaB**, **C10-OOD-Spat** and **C10-OOD-Sat**. Without the loss of generality, we can also curate four datasets each for a mentor based on C100 and IN images of a mentee.

**Adversarial Attack (AA) Errors.** Errors from adversarial images are specifically generated by adversarial attack methods to mislead or confuse the mentee. Given our assumption that the mentor has full access to the student model’s parameters, we focus exclusively on white-box adversarial attacks as they typically produce more subtle yet effective perturbations compared to their black-box counterparts. To generate adversarial images, we employ four untargeted adversarial attack methods: **PGD** (Madry et al., 2017) creates adversarial examples by repeatedly taking steps along the loss gradient; **CW** (Carlini & Wagner, 2017) attempts to minimize the  $L_2$  norm of the perturbation while ensuring misclassification. **Jitter** (Schwinn et al., 2023) adds Gaussian noise to the output logits to encourage a diverse set of target classes for the attack. **PIFGSM** (Gao et al., 2020) crafts patch-wise noise instead of pixel-wise noise. We set  $c = 1.0$  in the CW attack, and perturbation bound  $\epsilon = \frac{1}{255}$  for other attacks by default. See their papers for these hyper-parameter definitions. Intuitively, the attacks are stronger with higher hyper-parameter values; hence, the mentees make more mistakes.

Mentee	Error Source	CIFAR-10		CIFAR-100		ImageNet-1K		
		$N_{train}$	$N_{test}$	$N_{train}$	$N_{test}$	$N_{train}$	$N_{test}$	
ResNet50	ID	151/9547	151/151	773/7681	773/773	5967/32099	5967/5967	
		SpN	690/7930	690/690	1889/4333	1889/1889	9984/20048	9984/9984
	OOD	GaB	149/9553	149/149	760/7720	760/760	8013/25963	8012/8012
		Spat	222/9336	221/221	990/7032	989/989	7042/28874	7042/7042
		Sat	240/9282	239/239	1309/6072	1309/1309	8187/25439	8187/8187
		Jitter	338/8988	337/337	1054/6840	1053/1053	7591/27227	7591/7591
	AA	PGD	447/8661	446/446	1180/6460	1180/1180	9009/22973	9009/9009
		CW	487/8539	487/487	1120/6642	1119/1119	8102/25694	8102/8102
		PIFGSM	1613/5161	1613/1613	2090/3732	2089/2089	11226/16322	11226/11226
		ID	128/9618	127/127	675/7977	674/674	4733/35801	4733/4733
ViT	ID	286/9144	285/285	1155/6535	1155/1155	6019/31945	6018/6018	
		SpN	130/9610	130/130	678/7966	678/678	6402/30794	6402/6402
	OOD	GaB	170/9490	170/170	809/7573	809/809	5351/33947	5351/5351
		Spat	227/9319	227/227	1219/6345	1218/1218	5883/32351	5883/5883
		Sat	552/8344	552/552	1232/6304	1232/1232	10325/19025	10325/10325
		Jitter	649/8053	649/649	1410/5770	1410/1410	14960/11680	11680/11680
	AA	PGD	446/8664	445/445	1136/6592	1136/1136	8614/24158	8614/8614
		CW	799/7605	798/798	1812/4564	1812/1812	15038/11654	11654/11654
		PIFGSM						
		ID						

Table 1: **Dataset split for each error source used in mentor training.** If the mentor is trained on the mentee’s performance (ResNet50 or ViT) for a specific error source, the data in this error source will be split according to this table.  $N_{train}$  and  $N_{test}$  denote the number of training and testing samples, respectively, formatted as [number of samples misclassified by the mentee] / [number of samples correctly classified by the mentee].

Note that adversarial attacks are not always successful, and mentees can still correctly classify some adversarial images. We collect both the correctly and incorrectly classified adversarial images by a mentee based on C10 images, curating four datasets for the mentor: **C10-AA-PGD**, **C10-AA-CW**, **C10-AA-Jitter**, **C10-AA-PIFGSM**. Without the loss of generality, we can also curate four datasets each for a mentor based on C100 and IN images of a mentee.

**Training and Test Splits.** For any given dataset of a mentor, let  $N_c$  and  $N_w$  represent the sets of  $n$  correctly and  $m$  incorrectly classified images by a mentee. The sizes of  $N_c$  and  $N_w$  can vary significantly, depending on the mentee’s classification performance. A mentee with high recognition accuracy will have more correct classifications (big  $n$ ) and fewer incorrect ones (small  $m$ ). To create a balanced test set for a mentor, we select equal numbers of correctly and incorrectly classified samples. The remaining samples are used for training. The details of the dataset split are shown in **Tab. 1**. To address the long-tail problem in the training set, during each training epoch for a mentor, we randomly generate a batch of samples that includes an equal number of correctly and incorrectly classified images by the mentee.

**Evaluation Metric.** To assess the performance of mentors, we report their error prediction accuracy on the test set corresponding to each specified error source. For instance, a mentor trained on the C10-ID training set is evaluated on the C10-OOD-SpN test set. The error prediction accuracy is calculated by averaging the mentor’s accuracies on the samples that the mentee correctly classified and those that the mentee incorrectly classified. However, since a mentee can make mistakes across various real-world scenarios, a mentor must accurately predict errors across all error types. Therefore, we compute the average accuracy of a mentor across all test sets, including one ID error, four OOD errors, and four AA errors. For simplicity, we refer to this average accuracy across all nine error sources as **Accuracy**. A mentor randomly guessing whether a mentee’s image classification is correct or incorrect for a given image would achieve an accuracy of 50%.

## 4 RESULTS

### 4.1 TRAINING ON SPECIFIC ERRORS OF MENTEES IMPACTS THE PERFORMANCE OF MENTORS

A mentee’s mistakes can reveal their learning tendencies, behaviours, or traits. Here, we investigate which types of errors offer the most insight into understanding a mentee’s decision boundaries during image recognition tasks. We train mentors with identical architectures on datasets containing specific error types made by the mentee across C10 (**Fig. 3(a)**), C100 (**Fig. 3(b)**), and IN (**Fig. 3(c)**). For instance, if a mentor trained on C10-OOD achieves higher accuracy in error prediction compared to

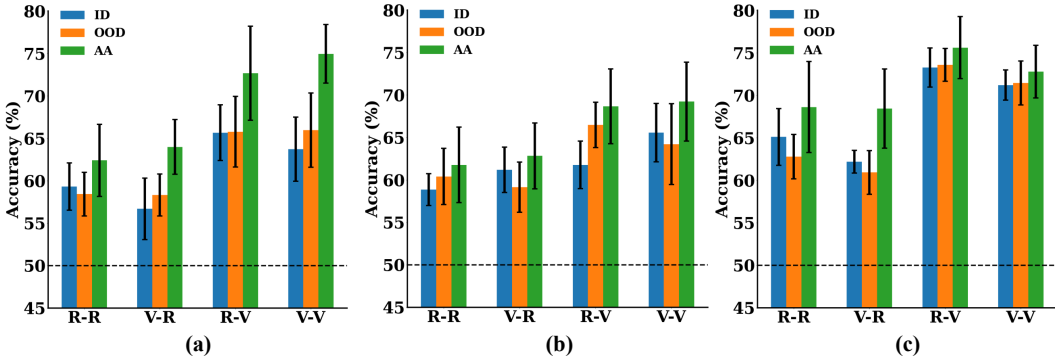


Figure 3: **Mentors trained on adversarial images of a mentee outperform mentors trained on OOD and ID images of the same mentee.** Average accuracy of a mentor trained on one type of error of a mentee for (a) CIFAR-10, (b) CIFAR-100 and (c) ImageNet-1K datasets is presented. Three types of errors made by a mentee are categorized based on in-domain (ID, blue), out-of-domain (OOD, orange), and images generated by adversarial attacks (AA, green). In each subplot, the labels on the x-axis are interpreted as [mentee]-[mentor], where ‘V’ and ‘R’ represent ViT and ResNet50 architectures for a mentee or a mentor respectively. Error bars indicate the standard deviation. The dotted black line indicates the chance level. See Sec. 3.3 for error types and the evaluation metric. The four sets of bars in each subfigure correspond to the heatmaps shown in subfigures (a), (b), (c), and (d) of Fig. S1- S3.

one trained on C10-IN, this suggests that in-domain errors provide less diagnostic information about the mentee’s decision-making process than out-of-domain errors. Both mentors and mentees may have the same or different backbones, such as ResNet50 (R) or ViT (V).

As shown in Fig. 3, over C10, C100, and IN images, the high accuracy for mentors trained on adversarial attack (AA) errors indicates that these errors offer deeper insights into the mentee’s decision process compared to out-of-domain (OOD) and in-domain (ID) errors. In some cases, mentors trained on OOD errors slightly outperformed those trained on ID errors, though both were still inferior to those trained on AA errors.

**Loss landscape analysis.** A loss landscape of a mentee reflects how a mentee’s loss function behaves across different parameter configurations. Mentors’ performance offers insights into the structure of a mentee’s loss landscape. Consistent with (Ilyas et al., 2019), the high accuracy of mentors trained on AA errors suggests that adversarial images lie closer to the mentee’s decision boundary, enabling more accurate prediction of the mentee’s mistakes and a deeper understanding of the loss landscape. Similarly, OOD data aids mentors in learning decision boundaries by shifting ID samples closer to the boundary. However, it does not explore the boundary as thoroughly as adversarial images. ID data, with fewer samples near the boundary, provides more limited exploration compared to adversarial examples.

## 4.2 MENTOR ARCHITECTURES MATTER IN ERROR PREDICTIONS

To computationally model the decision boundary of a mentee using a mentor, the mentor requires more complex architectures with a larger number of parameters than the mentee. Indeed, from Fig. 3, over all the datasets, we observed that utilizing ViT (V) as the mentor backbone consistently achieves higher accuracy across all error types of ViT-based and ResNet-based mentees compared to the mentor based on ResNet50 (R). One example of this performance disparity is observed in the context of the adversarial attack error type for CIFAR-10. The ViT-based mentor attains an accuracy of 74.95%, substantially higher than the accuracy of 63.99% for the ResNet-based mentor.

**Loss landscape analysis.** The performance difference between mentors’ architectures is due to ViT’s superior ability to identify features from error patterns. Its self-attention mechanism captures complex relationships among data samples, providing a deeper understanding of the mentee’s loss landscape, particularly in modelling irregular, rugged landscapes with sharp peaks and valleys.

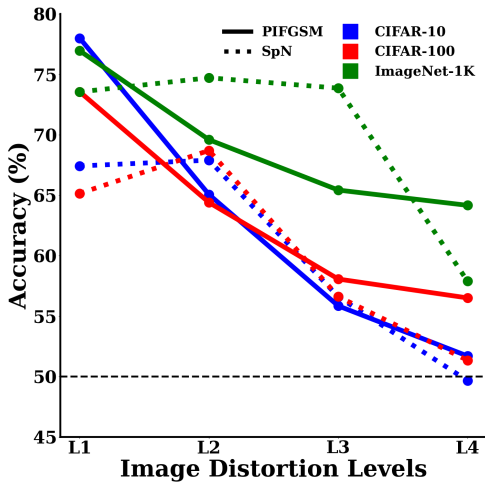


Figure 4: **A mentor’s accuracy is heavily influenced by the levels of image distortions introduced by out-of-domain perturbations and adversarial attacks.** ViT mentor’s accuracy is a function of varying image distortion levels from PIFGSM (Gao et al., 2020) and Speckle Noise (SpN) (Hendrycks & Dietterich, 2019) to the C10 images of a ResNet50-based mentee. The black dashed line indicates the chance level.

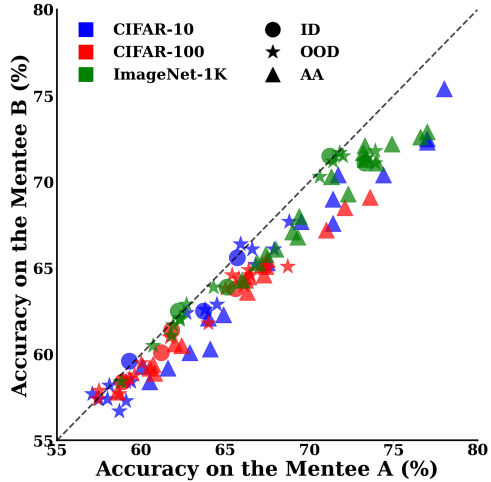


Figure 5: **Mentors can generalize their error predictions across different mentee architectures.** Mentors trained on mentee A’s predictions (x-axis) are evaluated against the predictions from mentee B (y-axis). Each marker is a generalization experiment of a mentor trained on different error types (marker shapes) in different image datasets (colours) of a mentee. The black dash line indicates the diagonal.

### 4.3 TRAINING ON IMAGES WITH SMALLER PERTURBATIONS HELPS ERROR PREDICTIONS

Although adversarial images have been demonstrated to aid in error prediction (Sec. 4.1), it remains unclear whether adversarial images with varying degrees of image distortion exhibit the same effect. A straightforward method to regulate the level of image distortion caused by adversarial attacks is to set the perturbation bound  $\epsilon$ . We employ four corruption levels by setting  $\epsilon = \frac{1}{255}, \frac{2}{255}, \frac{4}{255},$  and  $\frac{8}{255}$ . We use the adversarial attack PIFGSM as an example since the error patterns from PIFGSM are most effective for the mentor’s prediction (see Fig. S1- S3). As shown in Fig. 4, the mentor’s accuracy significantly decreases as the distortion level increases. In particular, for the C10-AA-PIFGSM, the accuracy at level 1 is 78.0%, which is notably higher than 51.7% at level 4. Our findings suggest that adversarial attacks employing smaller perturbations yield more benefits for mentor error prediction. This phenomenon can be attributed to the fact that adversarial images with minimal perturbations maintain closer proximity to the decision boundary of a mentee.

Building on the findings above, we investigate whether the mentor’s performance is influenced by how far OOD images are from the ID data. Specifically, we aim to determine whether the degree of deviation from the training domain impacts the mentor in a similar way to our observations on adversarial images. To explore this, we analyze images corrupted with Speckle Noise (SpN) and adjust the standard deviation  $\sigma$  of SpN to 0.01, 0.06, 0.15, and 0.6, representing four distinct levels of distortion. The outcomes are depicted in Fig. 4. We observe that the mentor’s accuracy improves as the distortion introduced by SpN decreases. For example, the mentor achieves an accuracy of 67.42% on level 1 of C10-OOD-SpN, while the accuracy drops significantly to 49.66% on level 4 of C100-OOD-SpN. This suggests that OOD error types with smaller perturbations enhance the mentor’s performance. However, unlike adversarial attacks, caution is necessary because the mentor’s accuracy can plateau with extremely small distortion levels, as shown by the minimal difference in accuracy between levels 1 and 2 of SpN in Fig. 4.

### 4.4 MENTORS GENERALIZE ACROSS MENTEES

In Sec. 4.1, mentors have demonstrated their ability to learn the error patterns of mentees. This observation raises an important question: can the error patterns learned from one mentee (mentee A) be generalized to another mentee (mentee B) when the two mentees employ different model



	ID	SpN	GaB	Spat	Sat	PGD	CW	Jitter	PIFGSM
R-R	59.3 ±2.8	59.1 ±3.1	58.1 ±2.2	59.4 ±2.1	57.1 ±1.9	60.5 ±2.2	61.6 ±2.7	60.1 ±2.6	67.5 ±4.1
V-R	56.7 ±3.6	57.5 ±2.8	59.1 ±1.6	58.0 ±3.4	58.7 ±1.2	64.9 ±2.7	64.1 ±3.0	62.9 ±3.8	64.0 ±3.0
R-V	65.7 ±3.3	67.9 ±4.4	62.7 ±3.1	66.6 ±2.8	65.9 ±4.3	71.4 ±5.5	69.5 ±4.6	71.7 ±4.2	78.0 ±3.5
V-V	63.7 ±3.8	64.5 ±3.5	63.8 ±3.2	66.8 ±4.5	68.8 ±4.3	77.0 ±2.6	71.4 ±2.6	74.4 ±2.4	77.0 ±2.6

Figure 6: **Our SuperMentor outperforms other mentor baselines on the CIFAR-10 dataset.** The row index follows the format [mentee]-[mentor], where 'V' and 'R' represent ViT and ResNet50 architectures for a mentee or a mentor respectively. The column index represents the error source used for training the mentor. Results in each cell denote the average error prediction accuracy over all error types with the standard deviation over 3 runs. Our SuperMentor's accuracy is highlighted in red boxes. The detailed performance of all mentors on specific error types is depicted in Fig. S1.

	$L_d$	$L_a$	ID	OOD				AA				Average
				SpN	GaB	Spat	Sat	PGD	CW	Jitter	PIFGSM	
C10	✗	✗	57.5	61.0	56.1	58.6	54.3	58.6	59.1	58.5	59.6	58.2
	✗	✓	80.0	73.7	79.2	77.9	74.3	80.5	76.5	79.7	71.2	77.0
		ours	80.9	73.2	80.5	79.4	75.6	81.4	78.2	80.7	71.9	78.0
C100	✗	✗	56.8	59.5	56.6	57.8	53.7	57.7	57.3	57.3	57.1	57.1
	✗	✓	75.0	70.9	74.8	74.1	68.1	78.1	75.2	76.2	66.5	73.2
		ours	75.4	71.1	75.4	74.5	68.4	78.3	75.6	76.6	66.9	73.6
IN	✗	✗	73.0	70.1	69.6	72.8	68.5	75.8	72.5	73.6	70.7	71.9
	✗	✓	78.7	73.1	73.6	78.0	73.2	83.0	78.4	79.9	72.2	76.7
		ours	78.9	73.6	74.6	78.3	73.6	83.0	78.4	79.9	72.3	77.0

Table 2: **Ablation study of loss components in SuperMentor.**  $L_d$  denotes the distillation loss (see Sec. 3.1) and  $L_a$  represents the alignment loss between the mentor's and mentee's predicted object class labels. SuperMentor is evaluated on the mistakes of a ResNet50-based mentee. Each result is the average of three independent runs. The performance of SuperMentor is coloured in grey. The full results with standard deviations are shown in Tab. S4.

architectures? To explore this, we evaluate all 324 mentors, whose performances are depicted in Fig. S1- S3, on the alternate mentee. Specifically, mentors trained on the errors of the ResNet50 mentee are tested on the predictions of the ViT mentee, and vice versa. The outcomes of these evaluations are illustrated in Fig. 5. Surprisingly, most points lie near the dashed diagonal line, implying that the mentors' performance does not significantly deteriorate when evaluated on the predictions of different mentee architectures. This finding indicates that ResNet50 and ViT mentees tend to produce similar error patterns when trained on the same dataset.

#### 4.5 OUR PROPOSED SUPERMENTOR MODEL OUTPERFORMS OTHER BASELINES

By drawing insights from observations in the subsections above, we propose an "oracle" mentor model, dubbed SuperMentor. We introduce the technical novelties of our SuperMentor below. First, as demonstrated in Sec. 4.1 and Sec. 4.3, mentors trained on adversarial images with small perturbations of a mentee outperform those trained on OOD and ID images; thus, our SuperMentor adopts the training data from the PIFGSM error source of mentees with  $\epsilon = \frac{1}{255}$ . Second, since ViT has been proven to be a more effective architecture for mentors than ResNet50 (Sec. 4.2), SuperMentor adopts ViT as the backbone architecture.

Fig. 6 shows that SuperMentor outperforms other baseline mentors in the CIFAR-10 dataset. The detailed performance of the SuperMentor, along with other baseline mentors on various error sources from the CIFAR-10, CIFAR-100 and ImageNet-1K datasets, is presented in Fig. S1- S3.

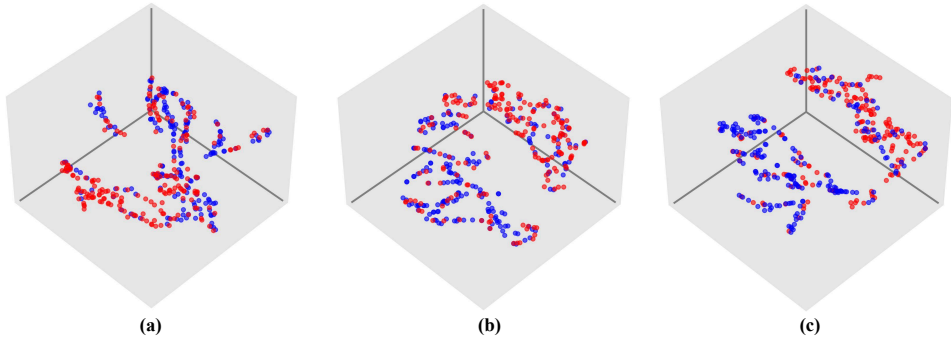


Figure 7: **3D visualization of the embeddings extracted from our SuperMentor Model for the classification of: a) C10-ID samples, b) C10-OOD-GaB samples and c) C10-AA-Jitter samples.** We use t-SNE (Van der Maaten & Hinton, 2008) to perform clusterings on the representations of our SuperMentor model for classifications of different error sources on the C-10 dataset. Red points indicate samples that the mentee fails to classify correctly, whereas blue points represent samples that the mentee successfully classifies. 200 red points and 200 blue points are randomly selected from the test sets and presented here. The visualized features are the embeddings computed based on the MLP in the second stream of the SuperMentor. Specifically, they are extracted before the final binary classification layer on whether the mentee makes a mistake.

We also present the visualization of the SuperMentor’s embeddings on three types of error sources of a mentee in **Fig. 7**. It is evident that SuperMentor can effectively segregate samples correctly classified by the mentee from those that are misclassified, forming two distinct clusters.

Next, we examine the effect of the distillation loss  $L_d$  (**Fig. 2**) on the SuperMentor performance. The results are presented in **Tab. 2**. It is clear that excluding  $L_d$  results in a decrease in SuperMentor’s accuracy across all datasets. For example, in the C10 dataset, the average accuracy of SuperMentor decreases from 78.0% to 58.2%. This suggests that  $L_d$  encourages SuperMentor to learn the fine-grained decision boundaries among different object classes of a mentee.

Alternatively, instead of utilizing the mentee’s logits, SuperMentor can incorporate an additional cross-entropy loss to align the mentor’s predicted object class labels with those of the mentee, denoted as  $L_a$ . From **Tab. 2**, we observe that replacing  $L_d$  with  $L_a$  leads to a slight decrease in accuracy. This is due to the fact that the mentee’s logits contain more information than the mentee’s class labels.

## 5 CONCLUSION

In our work, we tackle the challenge of predicting errors in AI models through extensive empirical evaluations using an end-to-end trainable "mentor" model. This mentor model is designed to assess the correctness of a mentee model’s predictions across three distinct error types: in-domain errors, out-of-domain errors, and adversarial attack errors. Our results show that the mentor model excels at learning from a mentee’s errors on adversarial images with minimal perturbations and, surprisingly, generalizes well to both in-domain and out-of-domain predictions of the same mentee. Additionally, we highlight the effectiveness of transformer-based mentor architectures compared to 2D-CNN-based ones, demonstrating their superior generalization capabilities across mentees with diverse backbones. Lastly, we introduce the SuperMentor, which significantly outperforms all existing mentor baselines.

Our work paves the way for several promising research directions in the field of safe and trustworthy AI. First, while our current research focuses on image classification, there is potential to extend this approach to other vision and language tasks, such as object detection and machine translation. Second, future research could explore mutual learning between mentors and mentees, where mentors not only learn from the mentee’s error patterns but also provide valuable feedback to help refine the mentee. Third, we can establish more rigorous evaluation criteria for mentors, broadening their predictive capabilities. For example, beyond predicting whether a mentee is likely to make errors, mentors could also forecast the specific types of errors a mentee may encounter. Fourth, this concept can be applied to investigate recognition errors in humans and primates, drawing parallels with AI models. Such analysis could provide insights into error pattern alignment between biological and artificial intelligent systems. Overall, our work lays the foundation for developing systems capable of anticipating the errors of others, offering practical value in high-stakes real-world applications.

## REFERENCES

- Mislav Balunović and Martin Vechev. Adversarial training and provable defenses: Bridging the gap. In *8th International Conference on Learning Representations (ICLR 2020)(virtual)*. International Conference on Learning Representations, 2020.
- Daniel Bogdoll, Maximilian Nitsche, and J Marius Zöllner. Anomaly detection in autonomous driving: A survey. In *Proceedings of the IEEE/CVF conference on computer vision and pattern recognition*, pp. 4488–4499, 2022.
- Azzedine Boukerche, Lining Zheng, and Omar Alfandi. Outlier detection: Methods, models, and classification. *ACM Computing Surveys (CSUR)*, 53(3):1–37, 2020.
- Wieland Brendel, Jonas Rauber, and Matthias Bethge. Decision-based adversarial attacks: Reliable attacks against black-box machine learning models. *arXiv preprint arXiv:1712.04248*, 2017.
- Nicholas Carlini and David Wagner. Towards evaluating the robustness of neural networks. In *2017 IEEE Symposium on Security and Privacy (SP)*, pp. 39–57. Ieee, 2017.
- Weilun Chen, Zhaoxiang Zhang, Xiaolin Hu, and Baoyuan Wu. Boosting decision-based black-box adversarial attacks with random sign flip. In *European Conference on Computer Vision*, pp. 276–293. Springer, 2020.
- Chih-Hong Cheng, Georg Nührenberg, and Hirotohi Yasuoka. Runtime monitoring neuron activation patterns. In *2019 Design, Automation & Test in Europe Conference & Exhibition (DATE)*, pp. 300–303. IEEE, 2019.
- Ching-Yao Chuang, Antonio Torralba, and Stefanie Jegelka. Estimating generalization under distribution shifts via domain-invariant representations. *arXiv preprint arXiv:2007.03511*, 2020.
- Khoi Tran Dang, Kevin Delmas, Jérémie Guiochet, and Joris Guérin. Can we defend against the unknown? an empirical study about threshold selection for neural network monitoring. *arXiv preprint arXiv:2405.08654*, 2024.
- Jia Deng, Wei Dong, Richard Socher, Li-Jia Li, Kai Li, and Li Fei-Fei. Imagenet: A large-scale hierarchical image database. In *2009 IEEE conference on computer vision and pattern recognition*, pp. 248–255. Ieee, 2009.
- Weijian Deng, Stephen Gould, and Liang Zheng. What does rotation prediction tell us about classifier accuracy under varying testing environments? In *International Conference on Machine Learning*, pp. 2579–2589. PMLR, 2021a.
- Zhijie Deng, Xiao Yang, Shizhen Xu, Hang Su, and Jun Zhu. Libre: A practical bayesian approach to adversarial detection. In *Proceedings of the IEEE/CVF conference on computer vision and pattern recognition*, pp. 972–982, 2021b.
- Alexey Dosovitskiy. An image is worth 16x16 words: Transformers for image recognition at scale. *arXiv preprint arXiv:2010.11929*, 2020.
- Raul Sena Ferreira, Joris Guerin, Jeremie Guiochet, and Helene Waeselynck. Sena: Similarity-based error-checking of neural activations. In *ECAI 2023*, pp. 724–731. IOS Press, 2023.
- Lianli Gao, Qilong Zhang, Jingkuan Song, Xianglong Liu, and Heng Tao Shen. Patch-wise attack for fooling deep neural network. In *Computer Vision—ECCV 2020: 16th European Conference, Glasgow, UK, August 23–28, 2020, Proceedings, Part XXVIII 16*, pp. 307–322. Springer, 2020.
- Ian J Goodfellow, Jonathon Shlens, and Christian Szegedy. Explaining and harnessing adversarial examples. *arXiv preprint arXiv:1412.6572*, 2014.
- Sven Gowal, Chongli Qin, Po-Sen Huang, Taylan Cemgil, Krishnamurthy Dvijotham, Timothy Mann, and Pushmeet Kohli. Achieving robustness in the wild via adversarial mixing with disentangled representations. In *Proceedings of the IEEE/CVF Conference on Computer Vision and Pattern Recognition*, pp. 1211–1220, 2020.

- Federica Granese, Marco Romanelli, Daniele Gorla, Catuscia Palamidessi, and Pablo Piantanida. Doctor: A simple method for detecting misclassification errors. *Advances in Neural Information Processing Systems*, 34:5669–5681, 2021.
- Joris Gu erin, Kevin Delmas, Raul Ferreira, and J er mie Guiochet. Out-of-distribution detection is not all you need. In *Proceedings of the AAAI conference on artificial intelligence*, volume 37, pp. 14829–14837, 2023.
- Devin Guillory, Vaishaal Shankar, Sayna Ebrahimi, Trevor Darrell, and Ludwig Schmidt. Predicting with confidence on unseen distributions. In *Proceedings of the IEEE/CVF international conference on computer vision*, pp. 1134–1144, 2021.
- Hafsa Habebh and Suril Gohel. Machine learning in healthcare. *Current genomics*, 22(4):291, 2021.
- Kaiming He, Xiangyu Zhang, Shaoqing Ren, and Jian Sun. Deep residual learning for image recognition. In *Proceedings of the IEEE conference on computer vision and pattern recognition*, pp. 770–778, 2016.
- Dan Hendrycks and Thomas Dietterich. Benchmarking neural network robustness to common corruptions and perturbations. *arXiv preprint arXiv:1903.12261*, 2019.
- Dan Hendrycks and Kevin Gimpel. A baseline for detecting misclassified and out-of-distribution examples in neural networks. *arXiv preprint arXiv:1610.02136*, 2016.
- Geoffrey Hinton. Distilling the knowledge in a neural network. *arXiv preprint arXiv:1503.02531*, 2015.
- Yanjun Huang, Jiatong Du, Ziru Yang, Zewei Zhou, Lin Zhang, and Hong Chen. A survey on trajectory-prediction methods for autonomous driving. *IEEE Transactions on Intelligent Vehicles*, 7(3):652–674, 2022.
- Andrew Ilyas, Shibani Santurkar, Dimitris Tsipras, Logan Engstrom, Brandon Tran, and Aleksander Madry. Adversarial examples are not bugs, they are features. *Advances in neural information processing systems*, 32, 2019.
- Yiding Jiang, Vaishnavh Nagarajan, Christina Baek, and J Zico Kolter. Assessing generalization of sgd via disagreement. *arXiv preprint arXiv:2106.13799*, 2021.
- Daniel Kang, Deepti Raghavan, Peter Bailis, and Matei Zaharia. Model assertions for debugging machine learning. In *NeurIPS ML Sys Workshop*, volume 3, 2018.
- Soheil Kolouri, Aniruddha Saha, Hamed Pirsiavash, and Heiko Hoffmann. Universal litmus patterns: Revealing backdoor attacks in cnns. In *Proceedings of the IEEE/CVF Conference on Computer Vision and Pattern Recognition*, pp. 301–310, 2020.
- Alex Krizhevsky, Geoffrey Hinton, et al. Learning multiple layers of features from tiny images. 2009.
- Balaji Lakshminarayanan, Alexander Pritzel, and Charles Blundell. Simple and scalable predictive uncertainty estimation using deep ensembles. *Advances in neural information processing systems*, 30, 2017.
- Kimin Lee, Kibok Lee, Honglak Lee, and Jinwoo Shin. A simple unified framework for detecting out-of-distribution samples and adversarial attacks. *Advances in neural information processing systems*, 31, 2018.
- Da Li, Yongxin Yang, Yi-Zhe Song, and Timothy M Hospedales. Deeper, broader and artier domain generalization. In *Proceedings of the IEEE international conference on computer vision*, pp. 5542–5550, 2017.
- Jiayang Liu, Weiming Zhang, Yiwei Zhang, Dongdong Hou, Yujia Liu, Hongyue Zha, and Nenghai Yu. Detection based defense against adversarial examples from the steganalysis point of view. In *Proceedings of the IEEE/CVF Conference on Computer Vision and Pattern Recognition*, pp. 4825–4834, 2019.

- Weitang Liu, Xiaoyun Wang, John Owens, and Yixuan Li. Energy-based out-of-distribution detection. *Advances in neural information processing systems*, 33:21464–21475, 2020a.
- Yunfei Liu, Xingjun Ma, James Bailey, and Feng Lu. Reflection backdoor: A natural backdoor attack on deep neural networks. In *Computer Vision—ECCV 2020: 16th European Conference, Glasgow, UK, August 23–28, 2020, Proceedings, Part X 16*, pp. 182–199. Springer, 2020b.
- Ilya Loshchilov and Frank Hutter. Sgdr: Stochastic gradient descent with warm restarts. *arXiv preprint arXiv:1608.03983*, 2016.
- Ilya Loshchilov and Frank Hutter. Decoupled weight decay regularization. *arXiv preprint arXiv:1711.05101*, 2017.
- Omid Madani, David Pennock, and Gary Flake. Co-validation: Using model disagreement on unlabeled data to validate classification algorithms. *Advances in neural information processing systems*, 17, 2004.
- Aleksander Mańdry, Aleksandar Makelov, Ludwig Schmidt, Dimitris Tsipras, and Adrian Vladu. Towards deep learning models resistant to adversarial attacks. *stat*, 1050(9), 2017.
- Akib Mashrur, Wei Luo, Nayyar A Zaidi, and Antonio Robles-Kelly. Machine learning for financial risk management: a survey. *Ieee Access*, 8:203203–203223, 2020.
- Zachary Nado, Neil Band, Mark Collier, Josip Djolonga, Michael W Dusenberry, Sebastian Farquhar, Qixuan Feng, Angelos Filos, Marton Havasi, Rodolphe Jenatton, et al. Uncertainty baselines: Benchmarks for uncertainty & robustness in deep learning. *arXiv preprint arXiv:2106.04015*, 2021.
- Yao Qin, Nicholas Frosst, Sara Sabour, Colin Raffel, Garrison Cottrell, and Geoffrey Hinton. Detecting and diagnosing adversarial images with class-conditional capsule reconstructions. *arXiv preprint arXiv:1907.02957*, 2019.
- Ali Rahmati, Seyed-Mohsen Moosavi-Dezfooli, Pascal Frossard, and Huaiyu Dai. Geoda: a geometric framework for black-box adversarial attacks. In *Proceedings of the IEEE/CVF conference on computer vision and pattern recognition*, pp. 8446–8455, 2020.
- Leo Schwinn, René Raab, An Nguyen, Dario Zanca, and Bjoern Eskofier. Exploring misclassifications of robust neural networks to enhance adversarial attacks. *Applied Intelligence*, 53(17): 19843–19859, 2023.
- Vaishaal Shankar, Achal Dave, Rebecca Roelofs, Deva Ramanan, Benjamin Recht, and Ludwig Schmidt. Do image classifiers generalize across time? In *Proceedings of the IEEE/CVF International Conference on Computer Vision*, pp. 9661–9669, 2021.
- Wenbo Shao, Jun Li, and Hong Wang. Self-aware trajectory prediction for safe autonomous driving. In *2023 IEEE Intelligent Vehicles Symposium (IV)*, pp. 1–8. IEEE, 2023.
- Wenbo Shao, Boqi Li, Wenhao Yu, Jiahui Xu, and Hong Wang. When is it likely to fail? performance monitor for black-box trajectory prediction model. *IEEE Transactions on Automation Science and Engineering*, 2024.
- Yiyu Sun, Chuan Guo, and Yixuan Li. React: Out-of-distribution detection with rectified activations. *Advances in Neural Information Processing Systems*, 34:144–157, 2021.
- Yiyu Sun, Yifei Ming, Xiaojin Zhu, and Yixuan Li. Out-of-distribution detection with deep nearest neighbors. In *International Conference on Machine Learning*, pp. 20827–20840. PMLR, 2022.
- C Szegedy. Intriguing properties of neural networks. *arXiv preprint arXiv:1312.6199*, 2013.
- Jonathan Uesato, Brendan O’donoghue, Pushmeet Kohli, and Aaron Oord. Adversarial risk and the dangers of evaluating against weak attacks. In *International conference on machine learning*, pp. 5025–5034. PMLR, 2018.
- Laurens Van der Maaten and Geoffrey Hinton. Visualizing data using t-sne. *Journal of machine learning research*, 9(11), 2008.

- Huiyan Wang, Jingwei Xu, Chang Xu, Xiaoxing Ma, and Jian Lu. Dissector: Input validation for deep learning applications by crossing-layer dissection. In *Proceedings of the ACM/IEEE 42nd International Conference on Software Engineering*, pp. 727–738, 2020.
- Chulin Xie, Keli Huang, Pin-Yu Chen, and Bo Li. Dba: Distributed backdoor attacks against federated learning. In *International conference on learning representations*, 2019.
- Jingkang Yang, Kaiyang Zhou, Yixuan Li, and Ziwei Liu. Generalized out-of-distribution detection: A survey. *International Journal of Computer Vision*, pp. 1–28, 2024.
- Yaodong Yu, Zitong Yang, Alexander Wei, Yi Ma, and Jacob Steinhardt. Predicting out-of-distribution error with the projection norm. In *International Conference on Machine Learning*, pp. 25721–25746. PMLR, 2022.

## S1 DETAILED PERFORMANCE OF MENTORS ACROSS VARIOUS ERROR SOURCES

As mentioned in **Sec. 4.1**, the detailed results of mentors across various error sources for the CIFAR-10, CIFAR-100, ImageNet-1K datasets are shown in **Fig. S1**, **Fig. S2** and **Fig. S3** respectively.

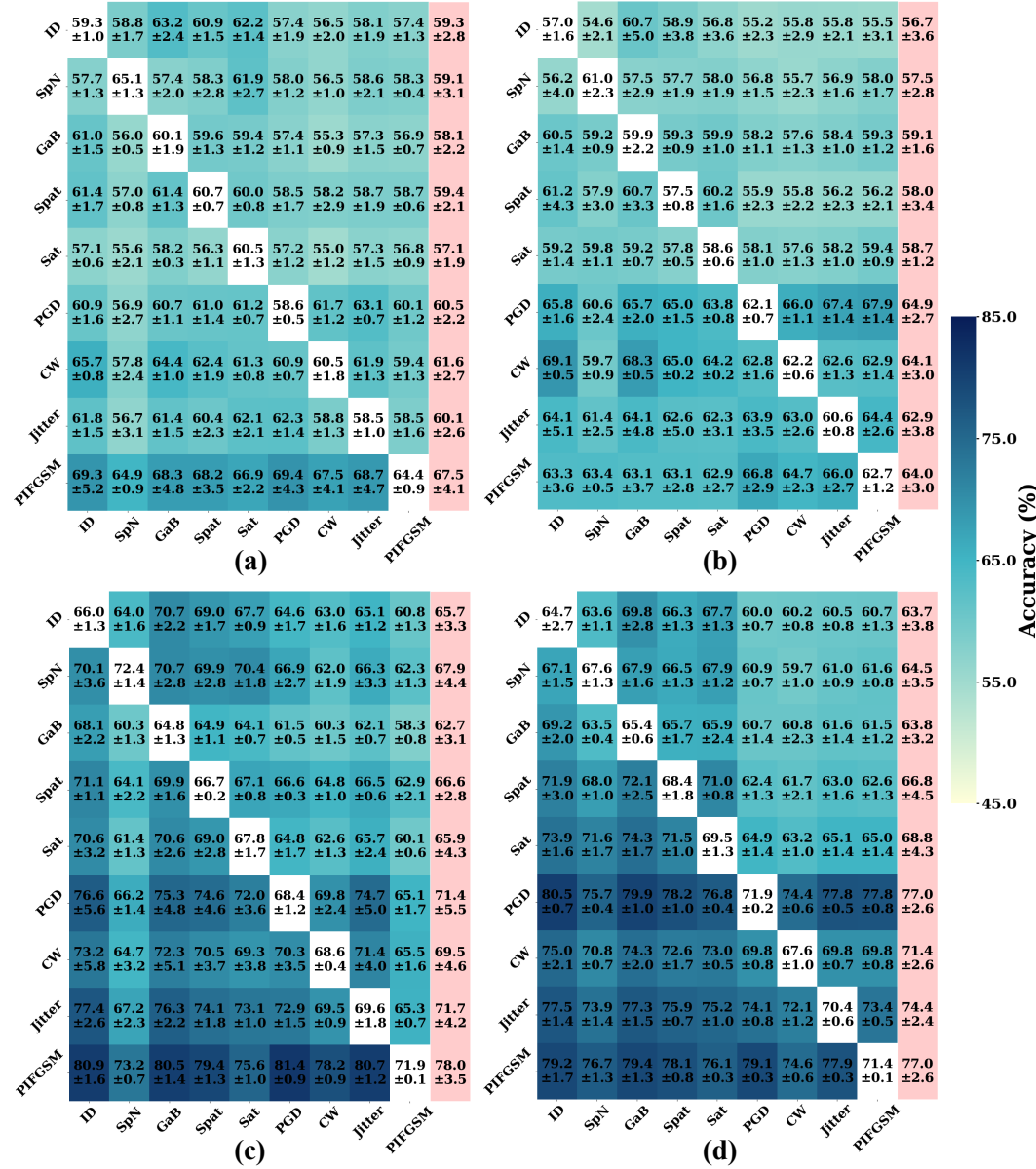


Figure S1: Heatmaps showing the average performance of mentor models across various error sources for the CIFAR-10 dataset, presented in the format [mentee]-[mentor]: a) ResNet50-ResNet50, b) ViT-ResNet50, c) ResNet50-ViT, and d) ViT-ViT. The heatmaps' row labels indicate the training error source for the mentor, while the column labels denote the testing error sources for the mentor. Results in each cell denote the average accuracy with the standard deviation over 3 runs. The pink-highlighted column displays the row-wise mean and standard deviation.

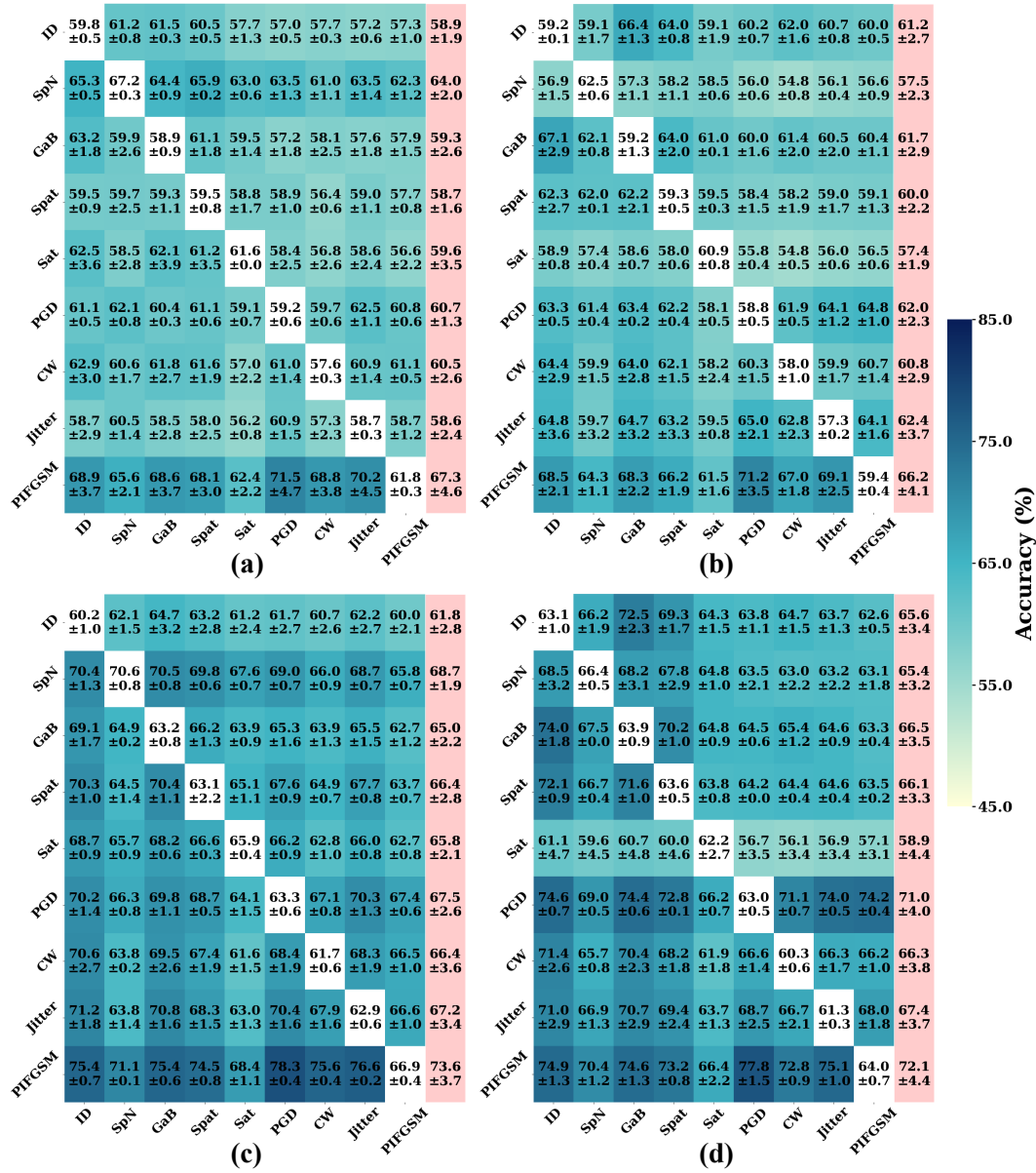


Figure S2: Heatmaps showing the average performance of mentor models across various error sources for the CIFAR-100 dataset, presented in the format [mentee]-[mentor]: a) ResNet50-ResNet50, b) ViT-ResNet50, c) ResNet50-ViT, and d) ViT-ViT. The heatmaps' row labels indicate the training error source for the mentor, while the column labels denote the testing error sources for the mentor. Results in each cell denote the average accuracy with the standard deviation over 3 runs. The pink-highlighted column displays the row-wise mean and standard deviation.



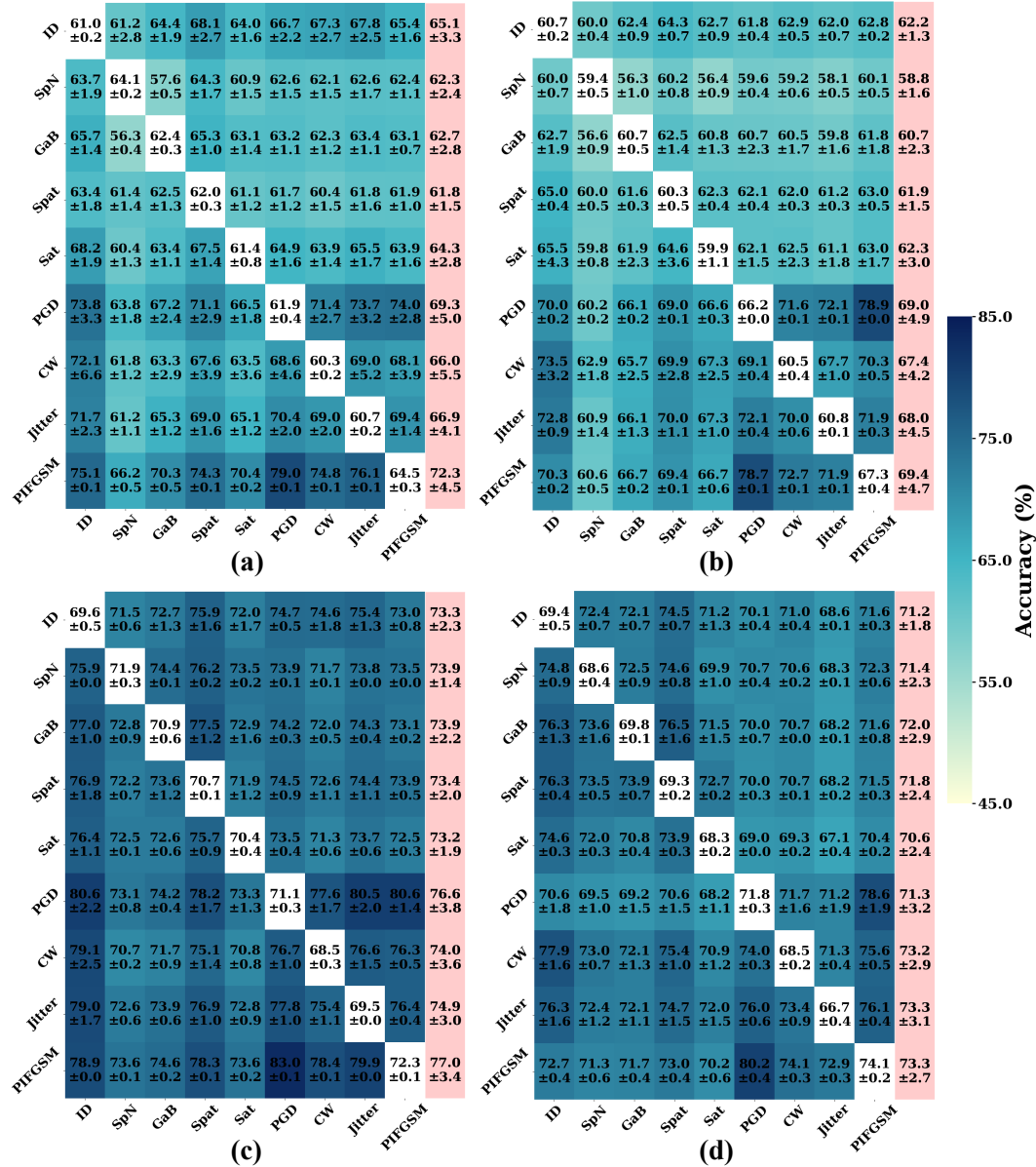


Figure S3: Heatmaps showing the average performance of mentor models across various error sources for the ImageNet-1K dataset, presented in the format [mentee]-[mentor]: a) ResNet50-ResNet50, b) ViT-ResNet50, c) ResNet50-ViT, and d) ViT-ViT. The heatmaps' row labels indicate the training error source for the mentor, while the column labels denote the testing error sources for the mentor. Results in each cell denote the average accuracy with the standard deviation over 3 runs. The pink-highlighted column displays the row-wise mean and standard deviation.

## S2 DETAILED PERFORMANCE OF MENTORS ACROSS MENTEE ARCHITECTURES

In **Fig. 5**, we show the generalization performance of mentors averaged over all three error types of mentees with various architectures. Here, we expand the results in the form of tables listing out all the individual accuracy for all the error sources on CIFAR-10, CIFAR-100 and ImageNet-1K datasets in **Tab. S1**, **Tab. S2**, and **Tab. S3** respectively.

Mentor		ResNet50		ViT	
Mentee		ResNet50→ ViT	ViT→ ResNet50	ResNet50→ ViT	ViT→ ResNet50
ID		59.3±2.8→ 59.6±2.0	56.7±3.6→ 54.5±2.4	65.7±3.3→ 65.6±3.4	63.7±3.8→ 62.5±3.0
OOD	SpN	59.1±3.1→ 58.4±3.3	57.5±2.8→ 57.4±2.1	67.9±4.4→ 66.1±5.0	64.5±3.5→ 62.9±2.7
	GaB	58.1±2.2→ 58.2±2.0	59.1±1.6→ 57.3±1.8	62.7±3.1→ 62.4±2.8	63.8±3.2→ 62.6±2.8
	Spat	59.4±2.1→ 58.4±2.1	58.0±3.4→ 57.4±3.0	66.6±2.8→ 66.1±3.7	66.8±4.5→ 65.2±3.8
	Sat	57.1±1.9→ 57.7±1.3	58.7±1.2→ 56.7±1.8	65.9±4.3→ 66.4±3.2	68.8±4.3→ 67.7±4.3
AA	PGD	60.5±2.2→ 58.4±1.5	64.9±2.7→ 62.3±1.7	71.4±5.5→ 69.0±4.5	77.0±2.6→ 72.3±4.1
	CW	61.6±2.7→ 59.2±2.2	64.1±3.0→ 60.3±2.0	69.5±4.6→ 67.7±4.0	71.4±2.6→ 67.6±3.1
	Jitter	60.1±2.6→ 59.3±1.8	62.9±3.8→ 60.1±3.3	71.7±4.2→ 70.4±3.5	74.4±2.4→ 70.4±3.8
	PIFGSM	67.5±4.1→ 65.3±3.4	64.0±3.0→ 62.1±2.3	78.0±3.5→ 75.4±3.4	77.0±2.6→ 72.5±3.9
Average		60.3±3.9→ 59.4±3.2	60.7±4.2→ 58.7±3.4	68.8±5.9→ 67.7±5.1	69.7±6.2→ 67.1±5.2

Table S1: **Detailed generalization performance of mentors across various mentee architectures on error sources from the CIFAR-10 dataset.** The mentee rows are formatted as [mentee A]→ [mentee B], as explained in **Fig. 5**. Results in each cell denote the average accuracy with the standard deviation over 3 runs.

Mentor		ResNet50		ViT	
Mentee		ResNet50→ ViT	ViT→ ResNet50	ResNet50→ ViT	ViT→ ResNet50
ID		58.9±1.9→ 58.4±1.8	61.2±2.7→ 60.1±2.1	61.8±2.8→ 61.4±2.9	65.6±3.4→ 63.8±2.0
OOD	SpN	64.0±2.0→ 61.8±3.5	57.5±2.3→ 57.9±2.9	68.7±1.9→ 65.1± 3.2	65.4±3.2→ 64.6±2.6
	GaB	59.3±2.6→ 58.6±2.0	61.7±2.9→ 61.0±1.9	65.0±2.2→ 63.8±2.5	66.5±3.5→ 64.6±1.9
	Spat	58.7±1.6→ 57.7±1.9	60.0±2.2→ 59.5±2.0	66.4±2.8→ 64.9±2.7	66.1±3.3→ 64.0±2.0
	Sat	59.6±3.5→ 58.8±3.4	57.4±1.9→ 57.4±2.6	65.8±2.1→ 64.4±3.0	58.9±4.4→ 58.4±4.4
AA	PGD	60.7±1.3→ 59.4±1.1	62.0±2.3→ 60.6±1.3	67.5±2.6→ 65.5±2.0	71.0±4.0→ 67.2±2.1
	CW	60.5±2.6→ 59.2±1.8	60.8±2.9→ 58.9±2.1	66.4±3.6→ 64.5±2.1	66.3±3.8→ 63.6±1.8
	Jitter	58.6±2.4→ 57.8±2.0	62.4±3.7→ 60.5±2.4	67.2±3.4→ 65.2±2.2	67.4±3.7→ 65.1±1.9
	PIFGSM	67.3±4.6→ 64.6±2.5	66.2±4.1→ 64.3±2.2	73.6±3.7→ 69.1±1.7	72.1±4.4→ 68.5±2.3
Average		60.8±3.9→ 59.6±3.2	61.0±3.8→ 60.0±2.9	66.9±4.1→ 64.9±3.2	66.6±5.2→ 64.4±3.6

Table S2: **Detailed generalization performance of mentors across various mentee architectures on error sources from the CIFAR-100 dataset.** The mentee rows are formatted as [menteeA]→ [menteeB], as explained in **Fig. 5**. Results in each cell denote the average accuracy with the standard deviation over 3 runs.

Mentor		ResNet50		ViT	
Mentee		ResNet50→ ViT	V→ ResNet50	ResNet50→ ViT	ViT→ ResNet50
ID		65.1±3.3→ 63.9±2.7	62.2±1.3→ 62.5±1.6	73.3±2.3→ 71.0±2.4	71.2±1.8→ 71.5±1.4
OOD	SpN	62.3±2.4→ 62.0±3.7	58.8±1.6→ 58.4±2.2	73.9±1.4→ 71.1±2.2	71.4±2.3→ 71.2±1.3
	GaB	62.7±2.8→ 62.9±3.8	60.7±2.3→ 60.5±2.7	73.9±2.2→ 71.8±3.0	72.0±2.9→ 71.5±1.7
	Spat	61.8±1.5→ 61.1±1.7	61.9±1.5→ 61.7±1.4	73.4±2.0→ 71.4±2.3	71.8±2.4→ 71.7±1.4
	Sat	64.3±2.8→ 63.9±3.5	62.3±3.0→ 62.1±2.7	73.2±1.9→ 71.2±2.6	70.6±2.4→ 70.3±1.2
AA	PGD	69.3±5.0→ 66.8±2.6	69.0±4.9→ 67.1±2.7	76.6±3.8→ 72.6±2.0	71.3±3.2→ 70.3±1.6
	CW	66.0±5.5→ 64.3±3.5	67.4±4.2→ 65.8±2.3	74.0±3.6→ 71.1±1.9	73.2±2.9→ 71.7±1.4
	Jitter	66.9±4.1→ 65.3±2.5	68.0±4.5→ 66.1±2.6	74.9±3.0→ 72.2±2.0	73.3±3.1→ 71.3±1.3
	PIFGSM	72.3±4.5→ 69.3±2.2	69.4±4.7→ 68.0±2.9	77.0±3.4→ 72.9±1.7	73.3±2.7→ 72.1±1.4
Average		65.6±5.0→ 64.4±3.8	64.4±5.1→ 63.6±3.9	74.4±3.0→ 71.7±2.4	72.0±2.8→ 71.3±1.5

Table S3: **Detailed generalization performance of mentors across various mentee architectures on error sources from the ImageNet-1K dataset.** The mentee rows are formatted as [menteeA]→ [menteeB], as explained in **Fig. 5**. Results in each cell denote the average accuracy with the standard deviation over 3 runs.

### S3 DETAILED RESULTS OF THE ABLATION STUDY ON THE LOSS COMPONENTS IN SUPERMENTOR

Extending the results shown in **Tab. 2**, we now include their standard deviations after 3 runs as presented in **Tab. S4**.

	$L_d$	$L_a$	ID	OOD				AA				Average
				SpN	GaB	Spat	Sat	PGD	CW	Jitter	PIFGSM	
C10	$\times$	$\times$	57.5± 1.2	61.0± 0.8	56.1± 1.1	58.6± 0.6	54.3± 1.5	58.6± 0.5	59.1± 1.2	58.5± 1.0	59.6± 0.6	58.2± 2.0
	$\times$	$\checkmark$	80.0± 1.8	73.7± 0.6	79.2± 2.0	77.9± 0.8	74.3± 1.9	80.5± 0.8	76.5± 0.8	79.7± 0.7	71.2± 0.4	77.0± 3.2
			ours	80.9± 1.6	73.2± 0.7	80.5± 1.4	79.4± 1.3	75.6± 1.0	81.4± 0.9	78.2± 0.9	80.7± 1.2	71.9± 0.1
C100	$\times$	$\times$	56.8± 1.2	59.5± 0.8	56.6± 1.1	57.8± 1.2	53.7± 1.3	57.7± 1.9	57.3± 1.9	57.3± 1.7	57.1± 0.5	57.1± 1.8
	$\times$	$\checkmark$	75.0± 0.7	70.9± 0.3	74.8± 0.7	74.1± 0.3	68.1± 0.8	78.1± 0.6	75.2± 0.6	76.2± 0.5	66.5± 1.0	73.2± 3.7
			ours	75.4± 0.7	71.1± 0.1	75.4± 0.6	74.5± 0.8	68.4± 1.1	78.3± 0.4	75.6± 0.4	76.6± 0.2	66.9± 0.4
IN	$\times$	$\times$	73.0± 4.2	70.1± 2.8	69.6± 3.1	72.8± 3.7	68.5± 3.4	75.8± 5.2	72.5± 4.2	73.6± 4.6	70.7± 0.5	71.9± 3.8
	$\times$	$\checkmark$	78.7± 0.1	73.1± 0.2	73.6± 0.5	78.0± 0.1	73.2± 0.3	83.0± 0.1	78.4± 0.1	79.9± 0.1	72.2± 0.2	76.7± 3.6
			ours	78.9± 0.0	73.6± 0.1	74.6± 0.2	78.3± 0.1	73.6± 0.2	83.0± 0.1	78.4± 0.1	79.9± 0.0	72.3± 0.1

Table S4: **Detailed results of the ablation study on the loss components in SuperMentor.**  $L_d$  denotes the distillation loss (see **Sec. 3.1**) and  $L_a$  represents the alignment loss between the mentor’s and mentee’s predicted class labels. SuperMentor is evaluated on a ResNet50 mentee. Results in each cell denote the average accuracy with the standard deviation over 3 runs. The performance of SuperMentor is highlighted in grey.